JGP Journal of General Physiology

RESEARCH ARTICLE

Rapid constriction of the selectivity filter underlies C-type inactivation in the KcsA potassium channel

Jing Li[1], Jared Ostmeyer[1], Luis G. Cuello[2], Eduardo Perozo[1], and Benoît Roux[1]

C-type inactivation is a time-dependent process observed in many K^+ channels whereby prolonged activation by an external stimulus leads to a reduction in ionic conduction. While C-type inactivation is thought to be a result of a constriction of the selectivity filter, the local dynamics of the process remain elusive. Here, we use molecular dynamics (MD) simulations of the KcsA channel to elucidate the nature of kinetically delayed activation/inactivation gating coupling. Microsecond-scale MD simulations based on the truncated form of the KcsA channel (C-terminal domain deleted) provide a first glimpse of the onset of C-type inactivation. We observe over multiple trajectories that the selectivity filter consistently undergoes a spontaneous and rapid (within 1–2 µs) transition to a constricted conformation when the intracellular activation gate is fully open, but remains in the conductive conformation when the activation gate is closed or partially open. Multidimensional umbrella sampling potential of mean force calculations and nonequilibrium voltage-driven simulations further confirm these observations. Electrophysiological measurements show that the truncated form of the KcsA channel inactivates faster and greater than full-length KcsA, which is consistent with truncated KcsA opening to a greater degree because of the absence of the C-terminal domain restraint. Together, these results imply that the observed kinetics underlying activation/inactivation gating reflect a rapid conductive-to-constricted transition of the selectivity filter that is allosterically controlled by the slow opening of the intracellular gate.

Introduction

A large class of K^+ channels displays a time-dependent phenomenon called C-type inactivation by which a reduction in the probability of the conductive state occurs upon prolonged activation (Hille, 2001). The functional coupling between activation and inactivation, a hallmark of K^+ channels, is of great physiological importance. For example, in neurons, the onset and duration of the conductive state of voltage-gated K^+ channels, which are directly modulated by the interplay of activation and inactivation, underlie the action-potential firing rates, and impaired inactivation can lead to a variety of neurological disorders (Aldrich et al., 1979; Roeper et al., 1997).

The pH-activated potassium channel from *Streptomyces lividans* (KcsA) has served as a critically important prototypical model system to identify the structural features associated with C-type inactivation at the molecular level (Blunck et al., 2006, 2008; Cordero-Morales et al., 2006, 2007; Cuello et al., 2010b). It is observed experimentally that KcsA inactivates within seconds after activation at low pH (Cordero-Morales et al., 2006, 2007; Chakrapani et al., 2011). There is strong evidence from functional data (Cordero-Morales et al., 2006, 2007; Chakrapani et al., 2011), x-ray crystallography (Zhou et al., 2001; Cuello et al., 2010a,b, 2017), NMR spectroscopy (Weingarth et al., 2014), and computations (Pan et al., 2011; Ostmeyer et al., 2013; Weingarth et al., 2014; Li et al., 2017) that the C-type inactivated state of the KcsA channel is associated with the constricted conformation of the selectivity filter. In particular, x-ray structures of the KcsA with the intracellular gate fully open showed that the inactivated state corresponds to a "constricted" conformation of the selectivity filter (Cuello et al., 2010a,b, 2017; Tilegenova et al., 2017).

The constricted conformation of the filter was first observed in a KcsA structure with a closed intracellular gate at low concentration of K^+ ions (PDB ID 1K4D; Zhou et al., 2001). By comparison to the canonical conductive filter (PDB ID 1K4C), this "low-K" conformation is characterized by a narrowing at the central glycine residue at position 77 at the center of the signature sequence TTVGYGD of the selectivity filter. Furthermore, water molecules bound behind the filter of the KcsA channel are indispensable to stabilize the constricted conformation (Ostmeyer et al., 2013; Weingarth et al., 2014). These water molecules must be released for the filter to return to a conductive conformation, explaining the long kinetics timescale to recover from C-type inactivation. Broadly emerging from these studies is the view that the con-

[1]Department of Biochemistry and Molecular Biology, University of Chicago, Chicago, IL; [2]Department of Cell Physiology and Molecular Biophysics, Texas Tech University Health Sciences Center, Lubbock, TX.

Correspondence to Benoît Roux: roux@uchicago.edu.

Table 1. **List of simulations for WT KcsA with different opening degrees of inner gate**

Traj ID	PDB[a]	Intracellular gate[b]	Runtime (ns)	Protonated residues	Ion concentration (mM)
1	3F7V[c]	Fully open (23 Å)	1,600	H25,E71,E120,H124	200
2	3F7V[c]	Fully open (23 Å)	340	H25,E71,E120,H124	150
3	3F7V[c]	Fully open (23 Å)	1,130	H25,E71,E120,H124	150
4	3F7V[c]	Fully open (23 Å)	450	H25,E71,E120	200
5	5VK6[d]	Fully open (22 Å)	10,000	H25,E71,E118,H124	150
6	3FB6	Partially open (16 Å)	500	H25,E71,E118	200
7	3FB6	Partially open (16 Å)	1,000	H25,E71,E120,H124	200
8	3FB6	Partially open (16 Å)	1,200	E71,E118	200
9	3FB5	Partially open (14 Å)	1,000	H25,E71,E120,H124	200
10	3FB5	Partially open (14 Å)	1,000	H25,E71	200
11	1K4C	Closed (11 Å)	1,500	E71	200
12	3FB6[e]	Partially open (17.5 Å)	110	H25,E71,E120	1,000
13	3F7V[e]	Fully open (23 Å)	190	H25,E71,E120,H124	1,000

[a]This is the crystal structure used as the initial conformation in MD simulations.
[b]The cross-subunit distance (shown in parentheses) between the Cα atoms of Thr112 of diagonally opposed monomer was used as an indicator for the opening degree of the inner gate in the initial conformation.
[c]To produce an open-conductive model from the 3F7V structure, which displays a constricted filter, the 2.0-Å resolution x-ray structure 1K4C was used as a template, and the filter was aligned to the channel using the backbone atoms of residues 65–74 and 80–84. The backbone atoms of the filter residues 74–80 have been restrained to maintain the conductive conformation in the initial phase of MD simulations. Video 1 shows the conformational transition in Traj-1 (0–800 ns).
[d]An alternative open-conductive model based on the open-conductive crystal structure 5VK6 for mutant E71A. In the initial conformation of this simulation, residue 71 was mutated back to Glu as the WT. In addition, the original disulfide bonds in the crystal structure were removed by mutating all of the relevant residues back to WT.
[e]These simulations were performed to test the permeability of partially opening inner gate. To collect enough sample within limited time, the ion concentration is higher than other simulations, and these are the only two trajectories with external electric field (300 mV). In addition, the initial conformations of Traj-12 and Traj-13 were snapshots, respectively, from Traj-6 and Traj-1, and the inner gate was restrained as 17.5 Å and 23 Å through the whole trajectory.

stricted conformation of the selectivity filter offers an accurate representation of the C-type inactivated state in KcsA.

Despite the progress, the conformational dynamics of the inactivation process remain poorly understood, and the structural underpinnings of C-type inactivation in the KcsA channel remain controversial (Devaraneni et al., 2013; Matulef et al., 2013, 2016; Liu et al., 2015; Li et al., 2017). This has even led some to openly question the functional significance of the constricted filter, arguing that it might correspond to a deep conformational state that becomes accessible only on a very long timescale during crystallization (Devaraneni et al., 2013; Matulef et al., 2013). To resolve these issues, it is essential to go beyond static x-ray structures with dynamical considerations (Li et al., 2017). Nonetheless, numerous questions remain unanswered regarding the activation/inactivation process in the KcsA channel, e.g., what controls the duration of the conductive period upon activation, is the conductive filter a long-lived metastable state upon opening of the intracellular gate, is the constricted filter physically and kinetically accessible within a microscopic timescale, and what are the factors modulating the interplay of activation and inactivation?

The goal of the present study is to elucidate the conformational dynamics of the inactivation process in the KcsA channel at the molecular level. To provide the maximum amount of information at the atomic level, a computational approach based on MD simulations is adopted here. The results from multiple MD trajectories and free energy calculations show that the selectivity filter of the KcsA channel remains conductive as long as the intracellular gate is not fully open, but that it undergoes a rapid and obligatory transition to a constricted nonconductive conformation on a microsecond timescale once the gate is fully open. In line with these computational results, macroscopic current recordings show that deletion of the C-terminal domain sharply increases the rate and extent of inactivation compared with the full-length KcsA channel, which is consistent with the fact that full-length KcsA is less open than the truncated form of the channel in a previous report because of the restraints of the C-terminal domain (Uysal et al., 2011; Dalmas et al., 2012). It is concluded that the long conduction period observed experimentally corresponds to long-lived states of the channel with an activation gate that is partially open.

Materials and methods

Atomic models of the WT KcsA were constructed based on crystal structures, i.e., PDB IDs 1K4C (Zhou et al., 2001), 3FB5 (Cuello et al., 2010b), 3FB6 (Cuello et al., 2010b), and 3F7V (Cuello et al., 2010b), which represent a spectrum of structural states with the

inner gate closed, partially open, and fully open. The selectivity filter is conductive in crystals structures 1K4C, 3FB5, and 3FB6, but constricted in 3F7V. The computational study was performed before a high-resolution x-ray structure of the inactivated channel with open gate recently became available (Cuello et al., 2017). To produce a fully open/conductive model from the 3F7V structure, the 2.0-Å resolution x-ray structure 1K4C was used as a template. The filter was aligned to the channel using the backbone atoms of residues 65–74 and 80–84 such that the backbone atoms of the filter residues 74-80 could be used as target coordinates for harmonic positional restraints (force constant 100 kcal/mol^{-1}). Once the filter coordinates matched that of 1K4C, K^+ ions were swapped into the filter at positions S0, S2, and S4, respectively, with a water molecule in between. The restraints on the filter were then linearly scaled to zero over a period of 10 ns during the final stages of equilibration. The transmembrane α-helices TM1 and TM2, incomplete in 3F7V, were extended to obtain a construct comprising residues 22 to 124. After energy minimization, the conductive filter was restrained for 50–100 ns to relax any unfavorable contacts destabilizing the filter. The conformational change of the selectivity filter was monitored by following the cross-subunit distance between the Gly77 Cα atoms of the two pairs of diagonally opposed monomers.

For all MD simulations, the channel was embedded in a bilayer of 3POPC:1POPG lipids and solvated in 150 mM or 200 mM KCl using the web service CHARMM-GUI (Jo et al., 2008, 2009). Most residues were assigned their standard protonation state at pH 7. The residue Glu71 is protonated to form a key hydrogen bond with Asp80 for the normal function of selectivity filter (Cordero-Morales et al., 2011; Bhate and McDermott, 2012), while His25, Glu118, Glu120, and His124 were protonated in different combinations to test the dynamics of activation gate. The total number of atoms in the MD systems is on the order of 41,000. The CHARMM force field PARAM36 for protein (MacKerell et al., 1998, 2004; Best et al., 2012), lipids (Klauda et al., 2010), and ions (Beglov and Roux, 1994) was used. Explicit water was described with the TIP3P model (Jorgensen et al., 1983). The models of KcsA were refined using energy minimization for at least 2,000 steps, and the ions and nonfilter backbone atoms were kept fixed throughout the minimization procedure. All the simulations were performed under NPT (constant number of particle N, pressure P, and temperature T) conditions at 310 K and 1 atm, and periodic boundary conditions with electrostatic interactions were treated by the particle mesh Ewald method (Darden et al., 1993) and a real-space cutoff of 12 Å. The simulations use a time step of 2 fs, with bond distances involving hydrogen atoms fixed using the SHAKE algorithm (Ryckaert et al., 1977). After minimization and equilibration with harmonic positional restraints on all of the Cα atoms, the equilibrated systems were simulated either using NAMD version 2.11 (Phillips et al., 2005) or on the special purpose computer Anton (Pittsburgh Supercomputer Center; Shaw et al., 2009). All of the equilibrium or nonequilibrium simulations performed for this study were summarized in Table 1.

Two sets of two-dimensional potential of mean force (2D-PMF) calculations were performed in two states, respectively, with partially open (~15 Å) and fully open (~23 Å) gates. The 2D-PMFs (see Fig. 4) with respect to the two coordinates were

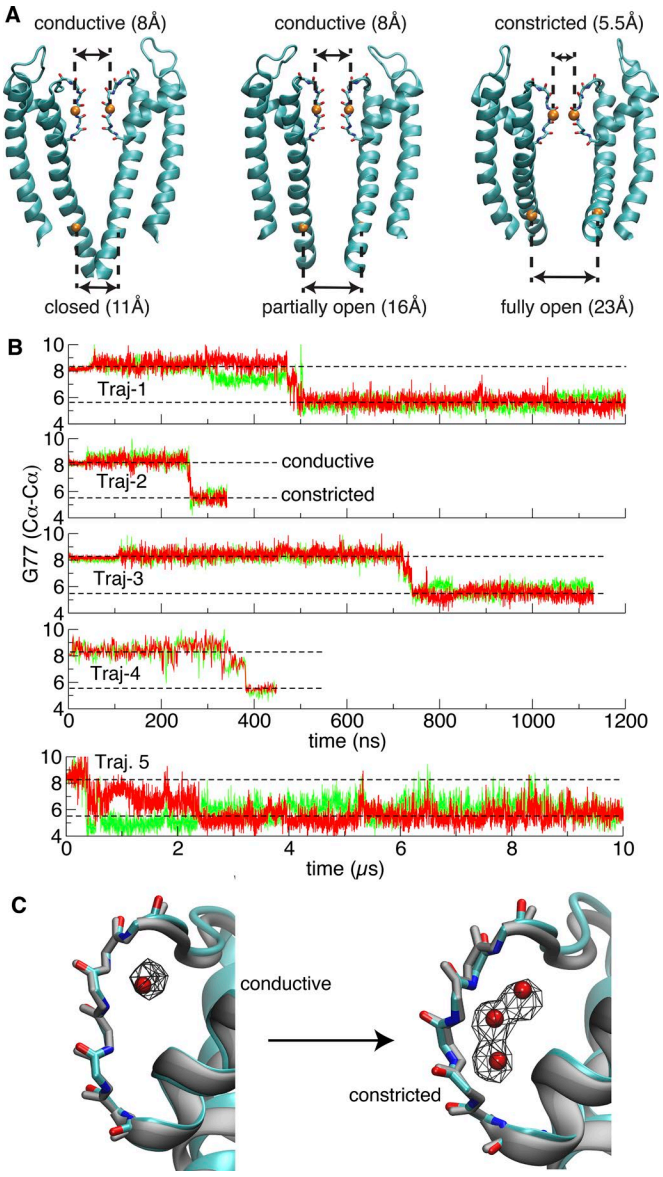

Figure 1. **The conformational indicators for the selectivity filter and the intracellular gate, and spontaneous constriction of the selectivity filter with fully open intracellular gate. (A)** The selectivity filter and the intracellular gate with distinct opening degrees in major functional states. The orange spheres represent Cα atoms of Gly77 and Thr112. The opening of the selectivity filter and the intracellular gate are, respectively, measured by the cross-subunit distance between the Cα atoms of Gly77 or Thr112 from diagonally opposed monomers. **(B)** Time series of the cross-subunit distance between the Cα atoms of Gly77 of diagonally opposed monomers A and C (red), and B and D (green) for five simulations started from the fully open crystal structures (3F7V and 5VK6). Two levels representing conductive and constricted states are illustrated in dashed line (n.b., the trace of Traj-4 looks thinner because it was performed on Anton with frames saved less frequently). **(C)** Transition of the selectivity filter from a canonical conductive to a typical constricted conformation. Left: Overlay of a conductive snapshot (taken at 250 ns from Traj-1) with the x-ray structure 1K4C of the KcsA channel with a closed intracellular gate (gray). Right: Overlay of a constricted structure (taken from the last snapshot of Traj-1) with the x-ray structure 1K4D of the KcsA channel at low K^+ with closed intracellular gate (gray). The red spheres indicate the position of the water oxygen in the crystal structures, and the wireframe represents the occupancy (50%) map of water molecules around the selectivity filter in either the conductive or constricted phase of Traj-1 with an open intracellular gate.

calculated using NAMD 2.11 (Phillips et al., 2005). One reaction coordinate r describes the width of the selectivity filter and is defined as the average cross-subunit distance between the Cα atoms of Gly77, whereas the other reaction coordinate z indicates the position of the external K^+ ion along the z axis relative to the center of the selectivity filter. The region of interest in the (r, z) space was covered by a grid of equally spaced umbrella sampling (US) windows. To improve the statistical sampling, the US calculations were performed using Hamiltonian replica-exchange MD (US/H-REMD; Sugita et al., 2000; Jiang et al., 2012). Some initial coordinates for the US windows were taken from the unbiased trajectories. Initial coordinates for the missing windows were obtained by driven MD simulations along the reaction coordinates to the space of the missing windows. Different from previous studies (Ostmeyer et al., 2013), there is no restraint on water molecules to access or leave the inactivating water binding site behind the selectivity filter. All of 85 windows were extended to 100 ns, and the total aggregate simulation time for the two sets of US/H-REMD calculations is 17 µs. Exchange attempts were made every 500 steps (or 1 ps of simulation of time), and neighboring windows were swapped if the Metropolis Monte Carlo exchange probability was satisfied. Windows were unbiased using the weighted histogram analysis method (Kumar et al., 1992; Roux, 1995), which only required that the US windows were generated according to Boltzmann statistics.

WT full-length and C-terminal domain–truncated KcsA (the C-terminal domain [35 amino acids] was removed by incubating the full-length channel with chymotrypsin (Sigma) in a 1:50 mass:mass ratio for 2 h, and then the truncated version of the WT channel was purified by size exclusion chromatography) were reconstituted at a 1:100 channel-to-lipid ratio (mass:mass), to obtain in a reliable way macroscopic currents recordings, in preformed Asolectin liposomes (Avanti Polar Lipids) that were made by sonicating a thin film of dried lipids in the following buffer: 200 mM KCl and 5 mM MOPS buffer (Sigma) at pH 7.0 (reconstitution buffer; Cortes et al., 2001). The mixture of KcsA (full-length or C-terminal–truncated) and liposomes (10 mg/ml of lipids) was incubated with Bio-Beads SM-2 (100–150 mg of wet beads; Bio-Rad) for an overnight period. Next day, the proteoliposome suspension was spun down at 100,000 *g* for 1 h. The resulting pellet was resuspended in 60 µl of reconstitution buffer. Next, 20-µl drops were placed on a microscope glass slide and dehydrated overnight in a desiccation chamber under constant vacuum. The next day, the samples were rehydrated by adding 20 µl of reconstitution buffer at 4°C overnight. After 24–48 h of rehydrating the sample, giant proteoliposomes were observed that were suitable for patch-clamp measurements, usually yielding robust macroscopic currents recordings. KcsA electrophysiological measurements were carried on in symmetrical 5-mM MOPS at the desired pH in the presence of 200 mM KCl. KcsA macroscopic current recordings were recorded from several independent experiments (n = 28 for the full-length and n = 38 for the C-terminal–truncated channel) with a patch-clamp amplifier Axopatch 200B, and currents were sampled at 10 kHz with an analogue filter set to 10 kHz. Patch pipettes, after fire polishing, displayed a resistance of 2.0 MΩ (they were filled with 200 mM KCl and 5 mM MOPS buffer at pH 4.0). KcsA macroscopic current recordings were analyzed with Clampfit 9.2, and the inactivation time constants were obtained by fitting single monoexponentials to the time-dependent decay of the current amplitude (Chakrapani et al., 2007).

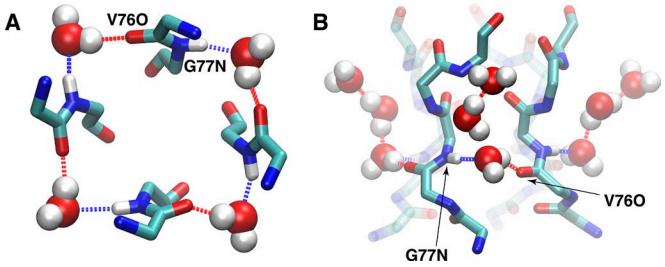

Figure 2. **Ring-like hydrogen bonding network to stabilize the constricted structure. (A and B)** Representative snapshot displaying this network formed by the buried water (van der Waals [vdW] representation) at the "bottom" site, Gly77 amide, and the carbonyl oxygen of Val76 from four subunits (stick representation), from bottom view (A), and side view (B).

Online supplemental material

Fig. S1 shows the comparison of the x-ray structure of the open-inactivated state (3F7V) with the open-conductive state for the noninactivating mutant E71A (5VK6) and the fluctuations from simulations. Fig. S2 shows the pathway for the entry of the inactivation water molecules behind the selectivity filter. Fig. S3 shows key contacts between the selectivity filter and TM2 for the allosteric coupling between gates in an open/constricted structure. Fig. S4 shows simulations results for the mutant F103A and I100A. Fig. S5 shows correlation between Thr74-Gly79 and Gly77-Gly77 distances during the conductive-to-constricted transition for the selectivity filter. Fig. S6 shows the dynamics of the inner gate during the simulations. Video 1 shows the conformational transition from Traj-1.

Results

Spontaneous filter constriction during MD simulations

C-type inactivation pertains to the time-dependent interconversion of the conductive selectivity filter toward a nonconductive state in response to an activating stimulus. To specifically model the KcsA channel in the functional state with an open intracellular gate and a conductive filter that (putatively) exists just after complete activation, two different approaches were used to build fully open structures with conductive filter for simulations. The first structure is based on the x-ray structure 3F7V with deleted C-terminal domain (residues 125–160) together with a conductive selectivity filter (substituted from the x-ray structure 1K4C). The second one is built based on a recently available crystal structure that represents a fully open/conductive conformation for the KcsA E71A mutant. All of the mutations in the latter structure were reverted back to WT, and the C-terminal is similarly truncated. The conformational state of the selectivity filter is monitored by following the cross-subunit distance between the Cα atoms of Gly77 from diagonally opposed monomers (Fig. 1 A): the distance is 5.5 Å for the constricted conformation and 8.1 Å for the conductive conformation (Zhou et al., 2001).

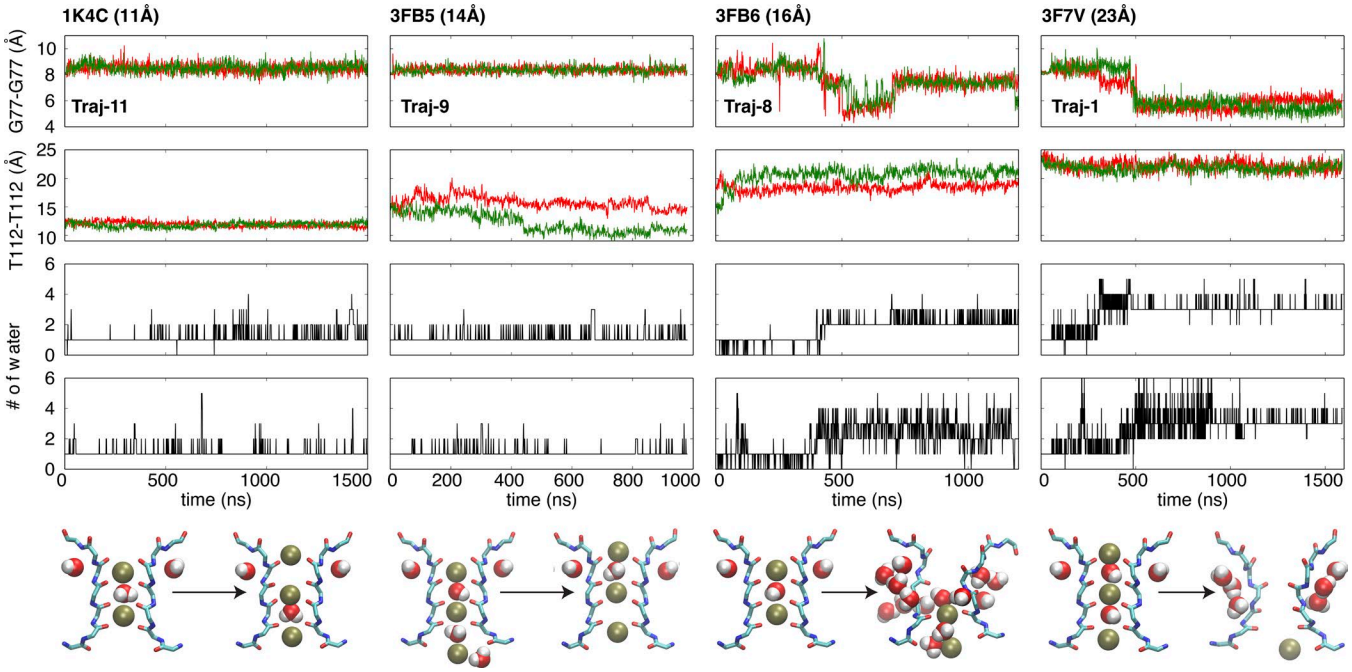

Figure 3. **The differentially conformational and dynamic behaviors of the selectivity filter of KcsA with various opening degrees of the intracellular gate.** Time series of the cross-subunit distance between the Cα atoms of Gly77 (first panel) or Thr112 (second panel) of diagonally opposed monomers A and C (red), and B and D (green), and the number of water behind the selectivity filter within subunit A (third panel) and B (fourth panel). Fifth panel: The first and last snapshots for the selectivity filter of corresponding trajectories. The backbone and the selectivity filter are represented as stick model, and both of ions and water molecules are in vdW representation. Only two opposite monomers are shown for clarity. Although multiple simulations have been performed as shown in the Table 1, here only a typical trajectory is selected from the same crystal structure, i.e., 1K4C (Traj-11), 3FB5 (Traj-9), 3FB6 (Traj-8), and 3F7V (Traj-1). In all cases, the K^+ concentration (0.15 or 0.2 M) is very similar to physiological condition.

As observed in Fig. 1 B, in all trajectories, the selectivity filter remains in the conductive state for a period of time until it spontaneously undergoes a rapid transition toward the constricted conformation. A similar conductive-to-constricted transition is consistently observed in the first four independent trajectories. Because the simulations of the channel with a conductive filter and open inner gate are based on models built from crystallographic structures, a legitimate question is whether the rapid constriction reflects a genuine conformational transition. In this regard, an important observation is that the filter remains conductive for at least 200–300 ns, indicating that the conformations represented by the models are genuinely metastable (Fig. 1). Furthermore, comparison of the x-ray structure of the open-inactivated state (3F7V) with the open/conductive state for the noninactivating mutant E71A (5VK6) shows that the backbone atoms have essentially the same coordinates in both structures, while simulations of the open/conductive state remain very close the x-ray open-conductive state (5VK6; Fig. S1). An additional simulation (Traj-5) started from an open/conductive structure (5VK6; E71A mutant has been reversed to WT) also constricts within 1 µs, albeit fluctuates longer than the first four trajectories. Following this transition, the selectivity filter remains stable in the constricted conformation.

As shown in Fig. 1 C, the conductive filter at the beginning of the trajectories is similar to that of the x-ray structure of KcsA with a closed intracellular gate (1K4C), and the constricted filter conformation after the conformational transition is similar to that of the low-K structure of KcsA with a closed intracellular gate (1K4D). Video 1 shows the conformational transition from Traj-1. To the best of our knowledge, these trajectories are the first displaying a spontaneous conductive-to-constricted filter transition of an open K^+ channel.

From the conductive-to-constricted transition, a small number of water molecules bound behind the filter of the KcsA channel spontaneously form four short water wires behind the selectivity filter. As shown in Fig. 1 C, these inactivating water molecules spontaneously occupy three locations, here referred to as top, middle, and bottom sites (Ostmeyer et al., 2013), which match precisely the position of three crystallographic water molecules in the KcsA low-K structure (1K4D) as well as in a recent high-resolution structure of the open-inactivated channel (Cuello et al., 2017). It is worth emphasizing that the simulations (Traj-1–4) were performed before the high-resolution structure was available. The overall pathway taken by the inactivating water molecules to reach their position behind the filter of each subunit can be visualized by backtracking their trajectory from these sites (Fig. S2). The binding of these three inactivating water molecules is indispensable to stabilize the constricted conformation (Ostmeyer et al., 2013; Weingarth et al., 2014). In contrast, a single water molecule occupies one location near the extracellular side when the filter is in the conductive conformation (Fig. 1 C), matching the position of one crystallographic water molecule in the KcsA structure (1K4C).

A notable aspect of the transitions is that all of the four subunits of the selectivity filter end up being occupied by the three inactivating water molecules at the same sites once they adopt the stable constricted conformation. The presence of a water

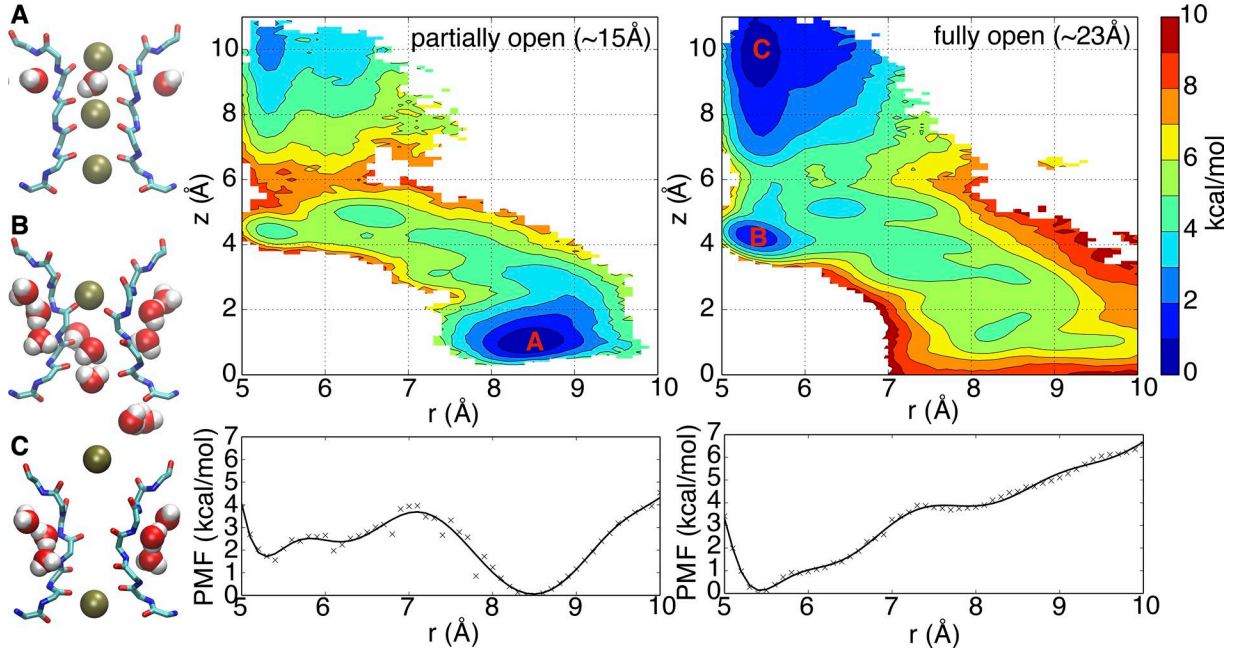

Figure 4. **2D-PMF to assess the conformational preferences of the selectivity filter with partially and fully open intracellular gate.** The horizontal reaction coordinate r describes the width of the selectivity filter and is defined as the average cross-subunit pinching distance between the Cα atoms of Gly77. The vertical reaction coordinate z indicates the position of the external K^+ ion along the z axis relative to the center of the selectivity filter. The lower panel is the one-dimensional PMF along horizontal reaction coordinate r, with integration of the vertical reaction coordinate z. The typical conformations (left) for three free energy basin are shown in stick for protein and vdW representation for both water and K^+ ion.

molecule at the bottom site behind one subunit facilitates the cooperative constriction of neighboring subunits, as shown from a close-up view in Fig. 2 that the buried inactivating water molecules and the protein form an extensive hydrogen bonding network. Namely, the water molecule occupying the bottom site forms hydrogen bonds with the Gly77 amide group within one subunit, and with the carbonyl oxygen of Val76 from the neighboring subunit. The hydrogen bond network significantly increases stability of the constricted conformation of the selectivity filter. The probability of both Gly77 amide and V76 carbonyl oxygen to form hydrogen bonds with water is above 60%, forming a stable ring-like hydrogen bond network among four subunits as shown in Fig. 2. In addition, more hydrogen bonds could be formed between the "bottom" water and E71 carbonyl oxygen, as well as the middle water and amide group from either Tyr78 or Gly79. All of these hydrogen bonds form a more complicated network to increase the free energy barrier substantially for the recovery of C-type inactivation.

The flipping of the carbonyl oxygen of Val76 to form a hydrogen bond with the water molecule is a key step for the conductive-to-constricted transition. It is notable that this carbonyl oxygen always coordinates a permeating K^+ ion when the filter adopts the canonical conductive conformation (1K4C). This phenomenon could be considered as a competitive inhibition of the K^+ ion binding in S2 and S3 sites by inactivating water. It provides explanations to why upon removal of external K^+ recovery from inactivation is slowed (Levy and Deutsch, 1996a,b; Gómez-Lagunas, 1997; Jäger et al., 1998), and the rate of C-type inactivation is decreased with increasing external K^+ in potassium channels (López-Barneo et al., 1993).

Filter constriction as a function of inner gate opening

To further explore the dynamical stability of the conductive selectivity filter, a series of microsecond-scale MD simulations were performed with various degrees of intracellular gate opening. The Cα–Cα cross-subunit distances of Thr112 along the second transmembrane helix TM2 (Fig. 1 A) is used to monitor the width of the intracellular gate (Cuello et al., 2010b). Channels with a closed (width of 11 Å), partially open (width of 14 and 16 Å), and fully open (width of 22 and 23 Å) intracellular gate were simulated (Table 1). Except structures with fully open intracellular gate mentioned above, the channel with the closed intracellular gate corresponds to the x-ray structure 1K4C, whereas the channel with a partially open intracellular gate is modeled on the basis of the x-ray structures 3FB5 and 3FB6. The results are shown in Fig. 3.

The unbiased MD trajectories show that the conformational propensity of the selectivity filter progressively shifts from conductive to constricted upon the opening of intracellular gate. As discussed above, the selectivity filter rapidly undergoes a spontaneous conductive-to-constricted transition when the intracellular gate is fully open (Traj-1). In contrast, the conductive conformation of the selectivity filter is extremely stable when the simulation is started with a closed intracellular gate (Traj-11). The selectivity filter maintains a stable conductive conformation when the intracellular gate is partially open with a width of 14 Å (Traj-9), whereas it displays larger fluctuations and twisted conformations when the intracellular gate is partially open with a width of 16 Å (Traj-8). In this case, the width of the intracellular gate expands slowly, as shown in the distances for pair of subunits stuck around 18 Å and 20 Å. Thus, the constricted confor-

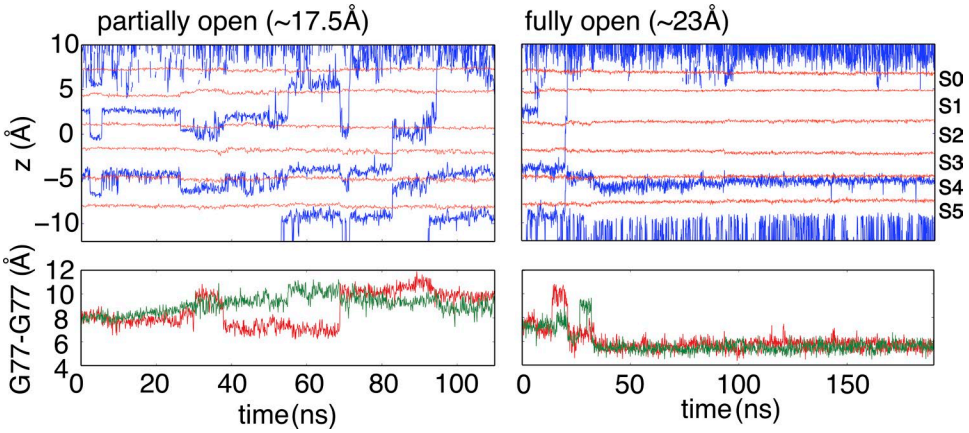

Figure 5. **Permeability of partially and fully open structures in the presence of external voltage (300 mV) and high K^+ ion concentration (1 M).** Top: Traces of K^+ ions (blue) are shown through the selectivity filter, and the average z coordinates of carbonyl oxygens of G79, Y78, G77, V76, and T75, and hydroxyl oxygen of T75 are respectively shown in red lines to indicate the position of K^+ binding sites. Bottom: Time series of the cross-subunit distance between the Cα atoms of Gly77 of diagonally opposed monomers. These simulations reveal that both the selectivity filter and intracellular gate are permeable for K^+ ions in a partially open structure, whereas the filter constricts (RMSD drops to 0.6 Å using 1K4D selectivity filter backbone as reference) in a fully open structure.

mation of the selectivity filter appears to be favored with a fully open intracellular gate, whereas the conductive conformation of the filter is preferred with a closed gate.

The conformational preference of the selectivity filter in the presence of a partially open intracellular gate is, however, more difficult to assess with confidence from such unbiased trajectories. 2D-PMFs were calculated using US/H-REMD simulations as a function of the Cα––Cα cross-subunit distance of Gly77 in the filter (r) and the position of the external K^+ ion along the pore axis (z). Controlling the K^+ ion in the US/H-REMD calculations is necessary for computational efficiency because its movements through the binding sites S0-S1-S2 is tightly coupled with the constricted-to-conductive transition of the filter (Ostmeyer et al., 2013). The 2D-PMF was determined for a partially open intracellular gate (15 Å) and a fully open intracellular gate (23 Å). In contrast from the restricted potential of mean force (PMF) previously reported (Ostmeyer et al., 2013), no restraint was applied on the inactivating water molecules to allow them to equilibrate over the different sites behind the filter.

The calculated 2D-PMFs shown in Fig. 4 clearly display the relative population shift of the conductive and constricted conformation as a function of intracellular gate opening. When the intracellular gate is only partially open, there is a local free energy basin around r = 8.5 Å, corresponding to the conductive state. In contrast, when the intracellular gate is fully open, there is a local free energy basin at r = 5.5 Å, corresponding to the constricted state. Thus, with a fully open intracellular gate, the selectivity filter would be expected to spontaneously transit from the conductive to the constricted conformation, as this process goes downhill on the free energy surface. These observations are consistent with the results from the unbiased simulations shown in Figs. 1 and 3 and also in agreement with single molecule fluorescence experiments on KcsA revealing that a small fraction of channels with an open intracellular gate were conductive (Blunck et al., 2006). It should be noted that the large free energy barrier of 6–7 kcal/mol in the 2D-PMF of the partially open channel (15 Å) pertains only to the constricted-to-conductive transformation of the filter and the binding of one K^+ ion; it does not correspond to the multi-ion translocation process that supports ion conduction (Medovoy et al., 2016).

Channel permeability in voltage-driven simulations

To ascertain the ion permeability of both partial and fully open structures, nonequilibrium MD simulations were performed in the presence of a transmembrane potential (300 mV). With the fully open gate (23 Å), the selectivity filter spontaneously constricted within 30 ns (Fig. 5), and no conduction event was observed after constriction, consistent with the equilibrium simulations (Fig. 1 B) and the PMF (Fig. 4). The ion concentration of these simulations was increased to 1 M to increase the number of permeation events. The selectivity filter in the fully open structure still constricts under such a high ion concentration, suggesting that gate opening has a dominant impact on the conformational preference of the selectivity filter. With the partially open gate (17 Å), 2 permeation events were observed within 100 ns, indicating that both the intracellular gate and the selectivity filter allow ion conduction. It is worth noting that Heer et al. (2017) recently argued on the basis of PMF calculations that the free energy barriers along the selectivity filter of the closed KcsA channel (1K4C) were too large to be compatible with the concept of rapid ion conduction, but the free energy barriers along the filter of the channel became smaller, and thus, more compatible with rapid ion conduction once the intracellular gate was opened. Although the notion of a nonconductive selectivity filter when the gate is closed is intriguing, it is important to keep in mind that the rate of ion permeation is exquisitely sensitive to the force field and that conclusion about free energy barriers from computational models must be considered with caution (Bernèche and Roux, 2001; Furini and Domene, 2009; Jensen et al., 2013; Köpfer et al., 2014; Medovoy et al., 2016; Heer et al., 2017). Whether at this point any of the current molecular mechanical force field is sufficiently accurate to quantitatively match experimental channel conductance is unclear. For this reason, we limit the present discussion to the conformational aspects of gating/inactivation in the KcsA channel.

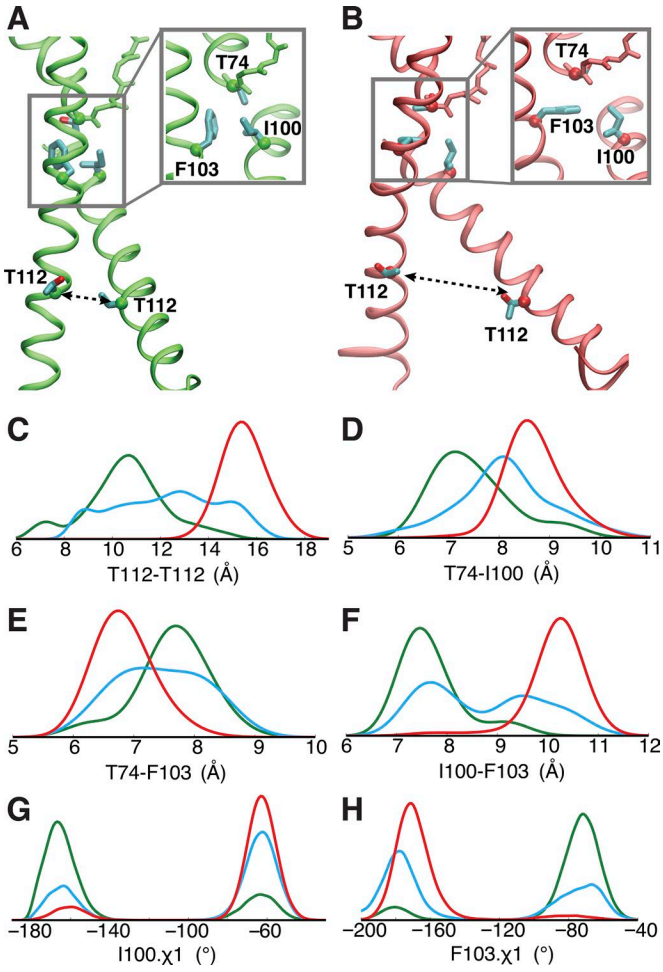

Figure 6. **Correlation between inner gate opening and local conformational rearrangement of Phe103, Ile100, and Thr74. (A and B)** Critical conformational difference between partially (A) and fully (B) open structure for the transmembrane helices and the selectivity filter. **(C–H)** Probability densities of three ensembles, respectively, were determined by combining several trajectories started from three crystal structures, i.e., two trajectories (Traj-9 and -10) started from 3FB5 (green), three trajectories (Traj-6–8) from 3FB6 (blue), and four trajectories (Traj-1–4) from 3F7V (red), to represent the opening degrees from partially to fully open of the inner gate. The probability density functions of these Cα-atom distances and rotamers were estimated by using kernel density estimation based on the sample distributions. In C, D, and F, the histograms correspond to the distances, i.e., T112-T112, T74-I100, and I100-F103, between adjacent subunits (as opposed to diagonally opposed cross-subunit distance discussed used elsewhere) because they yield a clearer picture for the allosteric coupling due to the key inter-subunit contacts from adjacent subunits.

Key residues responsible for allosteric coupling

Cross-talk between activation gate (intracellular gate) and inactivation gate (selectivity filter) was first revealed by EPR spectroscopy, where opening of the intracellular gate leads to subtle conformational changes in the pore helix and outer vestibule (Perozo et al., 1999; Cuello et al., 2010a). Based on a series of crystal structures, the allosteric coupling between the intracellular gate and the selectivity filter of the KcsA channel was characterized as a mechanical correlation between the degree of gate opening and ion occupancy of the selectivity filter (Cuello et al., 2010a,b, 2017). NMR studies provided further evidence that the activation/inactivation coupling is bidirectional (Baker et al., 2007; Imai et al., 2010; Wylie et al., 2014; Xu et al., 2017). Indeed, the coupling between two gates of voltage-activated channels has also been explained as a long-range allosteric (Panyi and Deutsch, 2006; Sadovsky and Yifrach, 2007). The present results indicate that the selectivity filter allows a stable conductive conformation for a partially open intracellular gate, up to a certain threshold, beyond which a conformational change toward the constricted state is triggered. The allosteric coupling between the selectivity filter and the intracellular gate arises from van der Waals contacts between the inner end of the selectivity filter (T74 and T75) and two residues located along the TM2 helix, Phe103 and Ile100 (Cuello et al., 2010a; Pan et al., 2011). Based on Figs. 3, 4, and 6, the threshold corresponds to a distance of 14 Å between the Thr112 of adjacent subunits (equivalent to 20 Å for the diagonally opposed subunits).

Examination of the current trajectories corresponding to different degrees of opening of the intracellular gate show a clear correlation between the opening of the intracellular gate and the local structural rearrangement in the vicinity of three critical residues: Thr74, Ile100, and Phe103 (Fig. 6). The analysis was performed to monitor the correlations among these critical structural elements by collecting the data from the current trajectories into three separate ensembles corresponding to different degrees of opening of the inner gate. The three ensembles capture a gradual widening of the inner gate from partially to fully open, as measured by the distance between the Cα of Thr112 from adjacent subunits along the TM2 helix (Fig. 6 C). The conditional probability distributions representing a gradual opening for the inner gate are shown in Fig. 6, C–H. As the inner gate progressively opens, the distance between Thr74 and Ile100 from neighboring subunits increases (Fig. 6 D), whereas the distance between Thr74 and Phe103 within the same subunit decreases (Fig. 6 E). Simultaneously, the distance between Phe103 and Ile100 increases (Fig. 6 F). A recent study suggests that a T75A single mutation could substantially change the inactivation property of KcsA and other potassium channels (Labro et al., 2018). Our analysis also reveals that the side chain of T75 forms tighter contact with I100 from the same subunit upon the opening of the intracellular gate (Fig. S3). The shifts in the distribution (Fig. 6, C–F; and Fig. S3) clearly show that the local structural rearrangement of Thr74, Thr75, Ile100, and Phe103 is coupled with the opening of the inner gate.

Because of the variations in the packing of Thr74, Thr75, Ile100, and Phe103 (Fig. 6, A and B), the rotameric state of Ile100 (Fig. 6 G) and Phe103 (Fig. 6 H) side chain is also affected by the opening of the intracellular gate. The bimodal distributions of the one-side chain dihedral angle for Ile100 and Phe103 suggest that both side chains can only adopt two orientations in the compact local environment. Upon the opening of the inner gate, there is a tighter contact between Thr74 and Phe103 (Fig. 6 E), and Thr75 and Ile100 (Fig. S3), and a looser contact between Ile100 and Phe103 (Fig. 6 F). As a result, the χ_1 side chain dihedral angle changes from −80 to −180° for Phe103 (Fig. 6 H), representing that its side chain reorients from parallel to perpendicular to the membrane normal (Fig. 6, A and B). The side chain of Ile100 also undergoes a similar reorientation (Fig. 6, A, B, and G).

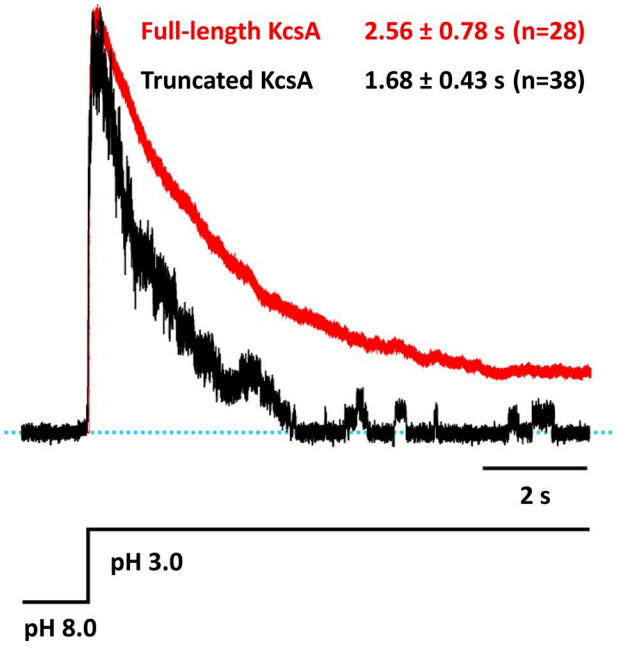

Figure 7. **Impact of KcsA activation gate opening in the absence/presence of the C-terminal domain on the degree of C-type inactivation.** Representative macroscopic current recordings elicited in response to switching the intracellular pH from 8.0 to pH 3.0 for the C-terminal–truncated (black trace) and full-length (red trace) KcsA. Inset: The time constant for C-type inactivation was obtained from single exponential fits of several independent macroscopic current recordings for the full-length (n = 28) and for the truncated form of KcsA (n = 38). The reported values are an average of the number (n) of independent experiments with the standard deviation (SD).

The existence of specific side chain rotamers for Ile100 and Phe103, and the direct van der Waals contacts with Thr74 and Thr75, demonstrate that the side chains clash with the inner end of the selectivity filter, thereby destabilizing the conductive conformation when the intracellular gate is open. These results are consistent with previous experiments and alchemical free energy computations indicating that the F103A and I100A mutations reduce inactivation (Cuello et al., 2010a; Pan et al., 2011). This hypothesis is further validated by additional unbiased MD simulations for two mutants, F103A and I100A. In contrast with the typical behavior of the WT KcsA channel (Fig. 1 B), the F103A and I100A mutants do not undergo a rapid constriction (Fig. S4).

The constriction of the filter is also strongly correlated with its length: the Thr74-Gly79 distance is reduced when the filter adopts a constricted conformation (Fig. S5). This observation suggests that factors stabilizing a short distance will promote inactivation. Indeed, mutations affecting the hydrogen bond between Glu71 and Asp80 strongly correlate with the propensity of the selectivity filter to inactivate. Accordingly, all mutations at the position of Glu71 (E71A, E71V, E71I) reduce inactivation, with the exception of E71H, which strongly promotes inactivation (Cordero-Morales et al., 2006, 2007). In the present study, the clash of Phe103 with Thr74, and Ile100 with Thr75, when the intracellular gate is open acts to shorten the filter in the presence of Glu71-Asp80 hydrogen bond. The conformational response of the filter to the TM2 pushing when the gate opens is a destabilization of the (long) conductive state relative to the (short) constricted conformation. This conformational rearrangement promoted by the opening of the intracellular gate is the structural basis of C-type inactivation (Cuello et al., 2010a,b, 2017; Ostmeyer et al., 2013).

Slow opening of the gate dictates the apparent inactivation rate

The conductive-to-constricted transitions from MD displayed in Fig. 1 all take place within 1 µs. These simulations are all based on the truncated form of the KcsA channel in which the channel C-terminal domain (residues 125–160) has been deleted by chymotrypsin. Previous experimental studies showed that deletion of the C-terminal domain increases the rate and extent of inactivation compared with the full-length KcsA channel (Cuello et al., 2010a; Uysal et al., 2011). This is recapitulated in Fig. 7, where it is observed that the macroscopic activation curve of the truncated KcsA channel decays to zero current and the inactivation time constant is 1.7 s, whereas the full-length KcsA only decays to ∼15% of the peak level and the inactivation time constant increases to 2.6 s. Fluorescence energy transfer experiments indicate that truncation of the C-terminal leads to a wider opening of the inner bundle gate upon activation compared with that of the full-length channel (Cuello et al., 2010a). Furthermore, according to x-ray structures and EPR, the inner gate diameter of the full-length channel is ∼21 Å (Uysal et al., 2011; Dalmas et al., 2012), smaller than with the truncated form of the channel (23 Å; Cuello et al., 2010a). This increased opening leads to a faster and deeper (smaller probability of being conductive) inactivation of the selectivity filter, as the restrictions on the degree of opening of the intracellular gate from the C-terminus domain are eliminated in the truncated channel. Thus, although the truncated channel is expected to inactivate faster than the full-length construct, the dynamical lifetime of the conductive filter in MD (Fig. 1) appears to be much too short to explain the periods of ion conduction observed experimentally (Fig. 7). The inconsistency suggests that other slow processes, presumably involving the intracellular gate, underlie the kinetics of the activation/inactivation of KcsA with the deleted C-terminal that is observed experimentally.

Trajectories started from a partially open intracellular gate (width of 14 Å and 16 Å in Fig. 3) provide additional insight on the timescale for the rearrangement of the intracellular gate. Remarkably, the width of the intracellular gate either remained essentially constant or deviated slightly over the course of these microsecond trajectories (Fig. S6). The slow timescale of the intracellular gate movements is in sharp contrast with the relative fast transitions of the selectivity filter observed in Fig. 1. Considering the potential impacts of the protonation for several critical titratable residues on the intracellular gate, different combinations of the protonation states were tested in simulations (Table 1). In all the trajectories, the width of the intracellular gate either remained constant or increased slightly by 2 Å. Importantly, the intracellular gate never reached a fully open state when starting from a partially open state, in accord with previous computational observations that there are two well-defined energy barriers separating the closed, partially open, and fully open states (Linder et al., 2013). The dynamic heterogeneity of the changes for the TM2 helices could slow down the par-

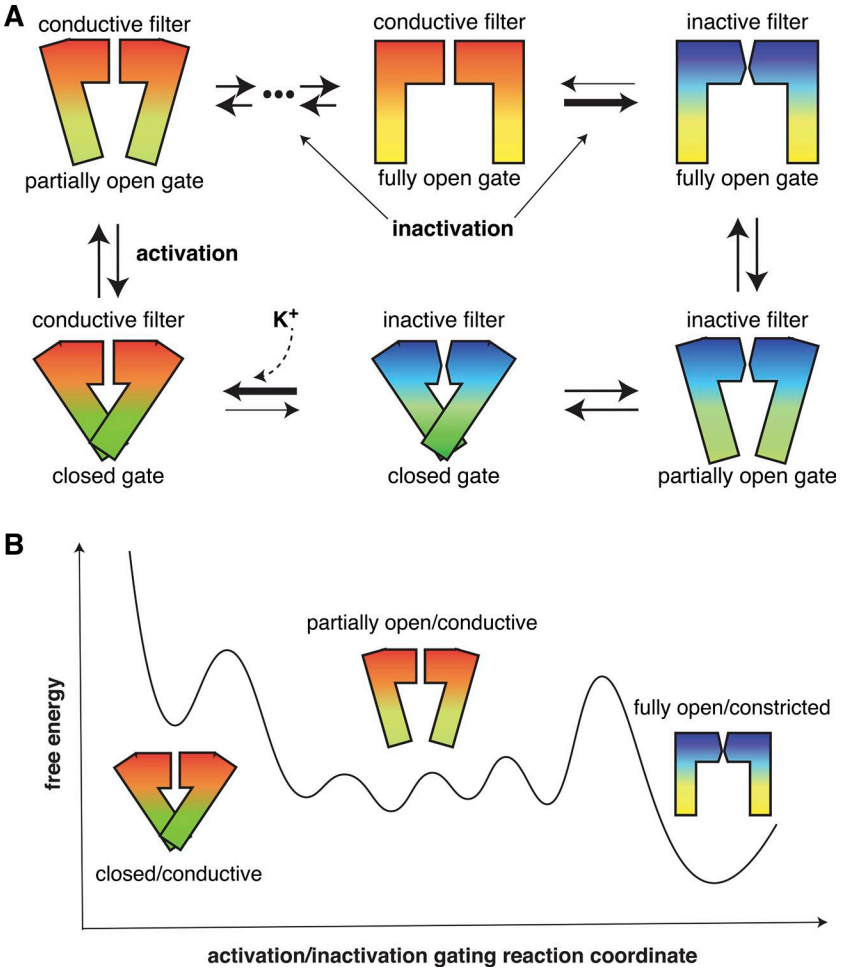

Figure 8. **Schematic depiction of functional cycle of KcsA, and hypothetic free energy profile along activation/inactivation gating reaction coordinate.** **(A)** Schematic depiction of the six dominant structural states. The thickness of horizontal arrows indicates the transition probability along the direction, whereas the thickness of vertical arrows is the same as the transition probability and is dependent on external stimulus. **(B)** Hypothetic free energy profile along activation/inactivation gating reaction coordinate in the presence of external stimulus, such as pH changing, for gate opening.

tially to fully open conformational rearrangement further, which might be much beyond the microsecond timescale. The fluctuations of the TM2 helices of the intracellular gate do not appear to be concerted (Fig. S6), suggesting that they are not tightly coupled. A single molecule fluorescence experiment detecting the movement of separate subunits of the KcsA channel revealed the opening of four subunits is a fairly slow motion that does not take place in a single concerted step (Blunck et al., 2006, 2008). Furthermore, independent EPR and NMR studies revealed that there is considerable conformational heterogeneity within the open states of KcsA, which is not visible in the available crystal structures (Dalmas et al., 2012; Kim et al., 2016). A solid-state NMR study also suggests that the open-conductive state for KcsA in cardiolipin bilayers at pH 4.0 mainly exists with a partially open activation gate (van der Cruijsen et al., 2017).

Discussion

As the KcsA channel inactivates within seconds after activation, the only way one can study such a slow process with MD simulations is by breaking it down into specific steps, and then studying each of those steps separately. To make progress, we started from the widely accepted paradigm, which breaks the activation/inactivation process into two main steps. In response to the external stimulus, there is a first transition (assumed rapid) of the channel from a closed to an open inner gate while the filter is in a conductive state, followed then by a second transition (assumed slow) toward a state with a constricted filter while the inner gate remains open. The goal of our computations was to examine the dynamics and thermodynamics of this putatively slow final step, where the long-lived metastable conductive filter collapses into a constricted conformation when the inner gate is open. To our surprise, the results from MD simulations and 2D-PMF calculations did not conform to the traditional view.

It appears that the selectivity filter can remain conductive as long as the intracellular gate is partially open, but rapidly converts to a constricted nonconductive conformation on a microsecond timescale once the intracellular gate is fully open. The calculated free energy landscapes in Fig. 4 show that the constricted filter is favored by a fully open gate (23 Å), whereas a conductive filter is favored by a partially open gate (15 Å). In accord with the 2D-PMFs, a spontaneous transition of the selectivity filter toward a constricted conformation was repeatedly observed within several hundred nanoseconds when the intracellular gate was fully open (Fig. 1 B). The transition of the tetrameric pore toward a fourfold symmetric constricted conformation occurs rapidly and cooperatively by virtue of a hydrogen bond network involving water molecules bound behind the selectivity filter (Fig. 2). Partially open states of the intracellular gate do not destabilize the conductive conformation of the selec-

tivity filter, which remains stable under these conditions (Figs. 3 and 4). Nonequilibrium simulations show that such a partially open intracellular gate allows the passage of K^+ ions through the TM2 helix bundle (Fig. 5). Once the intracellular gate is open beyond a certain threshold, however, steric clashes between the side chains of Phe103 and Ile100 along the TM2 helix and Thr74 and Thr75 at the inner end of the filter rapidly induce a conductive-to-constricted transition. The simulations also show that the dynamical rearrangements of the TM2 inner helices forming the intracellular gate take place very slowly, with multiple heterogeneous conformations.

The picture emerging from these results, illustrated schematically in Fig. 8, is that of a tighter allosteric coupling between the intracellular gate and the selectivity filter than commonly assumed (however, this view is in accord with a recent study [Tilegenova et al., 2017]). Constriction of the selectivity filter is under the direct control of the intracellular gate opening in the KcsA channel. The long-range allosteric coupling between the selectivity filter and the intracellular gate observed in the present study indicates that the selectivity filter cannot be stable for activation once the intracellular gate is fully open (width of 23 Å). Therefore, the ion conduction period observed experimentally must correspond to a channel conformation with an activation gate that is partially open (width of 16–20 Å). Once the intracellular gate is fully open, the conductive-to-constricted transition of the selectivity filter is rapid and obligatory. The short lifetime of the conductive filter with a fully open inner gate in the truncated form of the channel is inconsistent with the relatively long periods of sustained ion conduction observed experimentally (Fig. 7). This suggests that the macroscopically observed periods of ionic conduction should not predominantly correspond to channel conformations with a fully open activation gate. Based on these results, we propose that the experimentally observed ion conduction upon activation actually corresponds to conformations of the channel with a partially open intracellular gate, and the time to convert from a partially open to a fully open gate indirectly controls the rate of entry into inactivation. This is in contrast with a more traditional view of a functionally active channel with an open intracellular gate in which the conductive filter is assumed to be a long-lived metastable state. Although this conclusion was reached on the basis of simulations of the truncated form of the channel, there are reasons to believe that the same concept applies to other channels. For example, a slow fluorescence decay was observed in the voltage-activated Shaker channel that highly correlated with entry to the C-type inactivated state, and could be prevented by blocking the late transition to pore opening (Kalstrup and Blunck, 2013). Future work will aim to delineate the universal aspects of the activation/inactivation process in other channels.

Acknowledgments

The assistance of Lorenzo Pesce is acknowledged.

This research was supported by the National Institutes of Health through grants R01-GM062342 (B. Roux), R01-GM057846 (E. Perozo), R01-GM097159-01A1 (L.G. Cuello), and the Membrane Protein Structural Dynamics Consortium (U54-GM087519). Computer resources came from an allocation on Anton at the Pittsburgh Supercomputing Center provided by the National Center for Multiscale Modeling of Biological Systems through National Institutes of Health grant P41GM103712-1 and from a loan from D. E. Shaw Research, an allocation on the Blue Waters computer at the National Center for Supercomputing Applications from the National Science Foundation through grant PRAC-1640888, and the Beagle computer supported in part by the National Institutes of Health through resources provided by the Computation Institute and the Biological Sciences Division of the University of Chicago and Argonne National Laboratory, under grant 1S10OD018495-01.

The authors declare no competing interests.

Author contributions: J. Li, J. Ostmeyer, L. G. Cuello, E. Perozo, and B. Roux contributed to conception and design, acquisition of data, analysis, interpretation of data, and writing the manuscript.

José D. Faraldo-Gómez served as editor.

Submitted: 3 April 2018
Accepted: 12 July 2018

References

Aldrich, R.W. Jr., P.A. Getting, and S.H. Thompson. 1979. Mechanism of frequency-dependent broadening of molluscan neurone soma spikes. *J. Physiol.* 291:531–544. https://doi.org/10.1113/jphysiol.1979.sp012829

Baker, K.A., C. Tzitzilonis, W. Kwiatkowski, S. Choe, and R. Riek. 2007. Conformational dynamics of the KcsA potassium channel governs gating properties. *Nat. Struct. Mol. Biol.* 14:1089–1095. https://doi.org/10.1038/nsmb1311

Beglov, D., and B. Roux. 1994. Finite representation of an infinite bulk system: Solvent Boundary Potential for Computer Simulations. *J. Chem. Phys.* 100:9050–9063. https://doi.org/10.1063/1.466711

Bernèche, S., and B. Roux. 2001. Energetics of ion conduction through the K+ channel. *Nature.* 414:73–77. https://doi.org/10.1038/35102067

Best, R.B., X. Zhu, J. Shim, P.E. Lopes, J. Mittal, M. Feig, and A.D. Mackerell Jr. 2012. Optimization of the additive CHARMM all-atom protein force field targeting improved sampling of the backbone φ, ψ and side-chain χ(1) and χ(2) dihedral angles. *J. Chem. Theory Comput.* 8:3257–3273. https://doi.org/10.1021/ct300400x

Bhate, M.P., and A.E. McDermott. 2012. Protonation state of E71 in KcsA and its role for channel collapse and inactivation. *Proc. Natl. Acad. Sci. USA.* 109:15265–15270. https://doi.org/10.1073/pnas.1211900109

Blunck, R., J.F. Cordero-Morales, L.G. Cuello, E. Perozo, and F. Bezanilla. 2006. Detection of the opening of the bundle crossing in KcsA with fluorescence lifetime spectroscopy reveals the existence of two gates for ion conduction. *J. Gen. Physiol.* 128:569–581. https://doi.org/10.1085/jgp.200609638

Blunck, R., H. McGuire, H.C. Hyde, and F. Bezanilla. 2008. Fluorescence detection of the movement of single KcsA subunits reveals cooperativity. *Proc. Natl. Acad. Sci. USA.* 105:20263–20268. https://doi.org/10.1073/pnas.0807056106

Chakrapani, S., J.F. Cordero-Morales, and E. Perozo. 2007. A quantitative description of KcsA gating I: macroscopic currents. *J. Gen. Physiol.* 130:465–478. https://doi.org/10.1085/jgp.200709843

Chakrapani, S., J.F. Cordero-Morales, V. Jogini, A.C. Pan, D.M. Cortes, B. Roux, and E. Perozo. 2011. On the structural basis of modal gating behavior in K(+) channels. *Nat. Struct. Mol. Biol.* 18:67–74. https://doi.org/10.1038/nsmb.1968

Cordero-Morales, J.F., L.G. Cuello, Y. Zhao, V. Jogini, D.M. Cortes, B. Roux, and E. Perozo. 2006. Molecular determinants of gating at the potassium-channel selectivity filter. *Nat. Struct. Mol. Biol.* 13:311–318. https://doi.org/10.1038/nsmb1069

Cordero-Morales, J.F., V. Jogini, A. Lewis, V. Vásquez, D.M. Cortes, B. Roux, and E. Perozo. 2007. Molecular driving forces determining potassium channel slow inactivation. *Nat. Struct. Mol. Biol.* 14:1062–1069. https://doi.org/10.1038/nsmb1309

Cordero-Morales, J.F., V. Jogini, S. Chakrapani, and E. Perozo. 2011. A multipoint hydrogen-bond network underlying KcsA C-type inactivation. *Biophys. J.* 100:2387–2393. https://doi.org/10.1016/j.bpj.2011.01.073

Cortes, D.M., L.G. Cuello, and E. Perozo. 2001. Molecular architecture of full-length KcsA: role of cytoplasmic domains in ion permeation and activation gating. *J. Gen. Physiol.* 117:165–180. https://doi.org/10.1085/jgp.117.2.165

Cuello, L.G., V. Jogini, D.M. Cortes, A.C. Pan, D.G. Gagnon, O. Dalmas, J.F. Cordero-Morales, S. Chakrapani, B. Roux, and E. Perozo. 2010a. Structural basis for the coupling between activation and inactivation gates in K(+) channels. *Nature.* 466:272–275. https://doi.org/10.1038/nature09136

Cuello, L.G., V. Jogini, D.M. Cortes, and E. Perozo. 2010b. Structural mechanism of C-type inactivation in K(+) channels. *Nature.* 466:203–208. https://doi.org/10.1038/nature09153

Cuello, L.G., D.M. Cortes, and E. Perozo. 2017. The gating cycle of a K^+ channel at atomic resolution. *eLife.* 6:e28032. https://doi.org/10.7554/eLife.28032

Dalmas, O., H.C. Hyde, R.E. Hulse, and E. Perozo. 2012. Symmetry-constrained analysis of pulsed double electron-electron resonance (DEER) spectroscopy reveals the dynamic nature of the KcsA activation gate. *J. Am. Chem. Soc.* 134:16360–16369. https://doi.org/10.1021/ja3069038

Darden, T., D. York, and L. Pedersen. 1993. Particle Mesh Ewald: An n log (n) method for Ewald sums in large systems. *J. Chem. Phys.* 98:10089–10092. https://doi.org/10.1063/1.464397

Devaraneni, P.K., A.G. Komarov, C.A. Costantino, J.J. Devereaux, K. Matulef, and F.I. Valiyaveetil. 2013. Semisynthetic K^+ channels show that the constricted conformation of the selectivity filter is not the C-type inactivated state. *Proc. Natl. Acad. Sci. USA.* 110:15698–15703. https://doi.org/10.1073/pnas.1308699110

Furini, S., and C. Domene. 2009. Atypical mechanism of conduction in potassium channels. *Proc. Natl. Acad. Sci. USA.* 106:16074–16077. https://doi.org/10.1073/pnas.0903226106

Gómez-Lagunas, F. 1997. Shaker B K^+ conductance in Na+ solutions lacking K^+ ions: a remarkably stable non-conducting state produced by membrane depolarizations. *J. Physiol.* 499:3–15. https://doi.org/10.1113/jphysiol.1997.sp021907

Heer, F.T., D.J. Posson, W. Wojtas-Niziurski, C.M. Nimigean, and S. Bernèche. 2017. Mechanism of activation at the selectivity filter of the KcsA K^+ channel. *eLife.* 6:e25844. https://doi.org/10.7554/eLife.25844

Hille, B. 2001. Ionic Channels of Excitable Membranes. Third edition. Sinauer, Sunderland, MA.

Imai, S., M. Osawa, K. Takeuchi, and I. Shimada. 2010. Structural basis underlying the dual gate properties of KcsA. *Proc. Natl. Acad. Sci. USA.* 107:6216–6221. https://doi.org/10.1073/pnas.0911270107

Jäger, H., H. Rauer, A.N. Nguyen, J. Aiyar, K.G. Chandy, and S. Grissmer. 1998. Regulation of mammalian Shaker-related K^+ channels: evidence for non-conducting closed and non-conducting inactivated states. *J. Physiol.* 506:291–301. https://doi.org/10.1111/j.1469-7793.1998.291bw.x

Jensen, M.Ø., V. Jogini, M.P. Eastwood, and D.E. Shaw. 2013. Atomic-level simulation of current-voltage relationships in single-file ion channels. *J. Gen. Physiol.* 141:619–632. https://doi.org/10.1085/jgp.201210820

Jiang, W., Y. Luo, L. Maragliano, and B. Roux. 2012. Calculation of free energy landscape in multi-dimensions with hamiltonian-exchange umbrella sampling on petascale supercomputer. *J. Chem. Theory Comput.* 8:4672–4680. https://doi.org/10.1021/ct300468g

Jo, S., T. Kim, V.G. Iyer, and W. Im. 2008. CHARMM-GUI: a web-based graphical user interface for CHARMM. *J. Comput. Chem.* 29:1859–1865. https://doi.org/10.1002/jcc.20945

Jo, S., J.B. Lim, J.B. Klauda, and W. Im. 2009. CHARMM-GUI Membrane Builder for mixed bilayers and its application to yeast membranes. *Biophys. J.* 97:50–58. https://doi.org/10.1016/j.bpj.2009.04.013

Jorgensen, W.L., J. Chandrasekhar, J.D. Madura, R.W. Impey, and M.L. Klein. 1983. Comparison of simple potential functions for simulating liquid water. *J. Chem. Phys.* 79:926–935. https://doi.org/10.1063/1.445869

Kalstrup, T., and R. Blunck. 2013. Dynamics of internal pore opening in $K(_V)$ channels probed by a fluorescent unnatural amino acid. *Proc. Natl. Acad. Sci. USA.* 110:8272–8277. https://doi.org/10.1073/pnas.1220398110

Kim, D.M., I. Dikiy, V. Upadhyay, D.J. Posson, D. Eliezer, and C.M. Nimigean. 2016. Conformational heterogeneity in closed and open states of the KcsA potassium channel in lipid bicelles. *J. Gen. Physiol.* 148:119–132. https://doi.org/10.1085/jgp.201611602

Klauda, J.B., R.M. Venable, J.A. Freites, J.W. O'Connor, D.J. Tobias, C. Mondragon-Ramirez, I. Vorobyov, A.D. MacKerell Jr., and R.W. Pastor. 2010. Update of the CHARMM all-atom additive force field for lipids: validation on six lipid types. *J. Phys. Chem. B.* 114:7830–7843. https://doi.org/10.1021/jp101759q

Köpfer, D.A., C. Song, T. Gruene, G.M. Sheldrick, U. Zachariae, and B.L. de Groot. 2014. Ion permeation in K^+ channels occurs by direct Coulomb knock-on. *Science.* 346:352–355. https://doi.org/10.1126/science.1254840

Kumar, S., J.M. Rosenberg, D. Bouzida, R.H. Swendsen, and P.A. Kollman. 1992. The weighted histogram analysis method for free-energy calculations on biomolecules. I. the method. *J. Comput. Chem.* 13:1011–1021. https://doi.org/10.1002/jcc.540130812

Labro, A.J., D.M. Cortes, C. Tilegenova, and L.G. Cuello. 2018. Inverted allosteric coupling between activation and inactivation gates in K^+ channels. *Proc. Natl. Acad. Sci. USA.* 115:5426–5431. https://doi.org/10.1073/pnas.1800559115

Levy, D.I., and C. Deutsch. 1996a. Recovery from C-type inactivation is modulated by extracellular potassium. *Biophys. J.* 70:798–805. https://doi.org/10.1016/S0006-3495(96)79619-4

Levy, D.I., and C. Deutsch. 1996b. A voltage-dependent role for K^+ in recovery from C-type inactivation. *Biophys. J.* 71:3157–3166. https://doi.org/10.1016/S0006-3495(96)79509-7

Li, J., J. Ostmeyer, E. Boulanger, H. Rui, E. Perozo, and B. Roux. 2017. Chemical substitutions in the selectivity filter of potassium channels do not rule out constricted-like conformations for C-type inactivation. *Proc. Natl. Acad. Sci. USA.* 114:11145–11150. https://doi.org/10.1073/pnas.1706983114

Linder, T., B.L. de Groot, and A. Stary-Weinzinger. 2013. Probing the energy landscape of activation gating of the bacterial potassium channel KcsA. *PLOS Comput. Biol.* 9:e1003058. https://doi.org/10.1371/journal.pcbi.1003058

Liu, S., P.J. Focke, K. Matulef, X. Bian, P. Moënne-Loccoz, F.I. Valiyaveetil, and S.W. Lockless. 2015. Ion-binding properties of a K+ channel selectivity filter in different conformations. *Proc. Natl. Acad. Sci. USA.* 112:15096–15100. https://doi.org/10.1073/pnas.1510526112

López-Barneo, J., T. Hoshi, S.H. Heinemann, and R.W. Aldrich. 1993. Effects of external cations and mutations in the pore region on C-type inactivation of Shaker potassium channels. *Receptors Channels.* 1:61–71.

MacKerell, A.D.J., D. Bashford, M. Bellott, R.L. Dunbrack, J.D. Evanseck, M.J. Field, S. Fischer, J. Gao, H. Guo, S. Ha, et al. 1998. All-atom empirical potential for molecular modeling and dynamics studies of proteins. *J. Phys. Chem. B.* 102:3586–3616. https://doi.org/10.1021/jp973084f

MacKerell, A.D.J. Jr., M. Feig, and C.L. Brooks III. 2004. Improved treatment of the protein backbone in empirical force fields. *J. Am. Chem. Soc.* 126:698–699. https://doi.org/10.1021/ja036959e

Matulef, K., A.G. Komarov, C.A. Costantino, and F.I. Valiyaveetil. 2013. Using protein backbone mutagenesis to dissect the link between ion occupancy and C-type inactivation in K^+ channels. *Proc. Natl. Acad. Sci. USA.* 110:17886–17891. https://doi.org/10.1073/pnas.1314356110

Matulef, K., A.W. Annen, J.C. Nix, and F.I. Valiyaveetil. 2016. Individual ion binding sites in the K+ channel play distinct roles in C-type inactivation and in recovery from inactivation. *Structure.* 24:750–761.

Medovoy, D., E. Perozo, and B. Roux. 2016. Multi-ion free energy landscapes underscore the microscopic mechanism of ion selectivity in the KcsA channel. *Biochim. Biophys. Acta.* 1858(7 pt B):1722–1732. https://doi.org/10.1016/j.bbamem.2016.02.019

Ostmeyer, J., S. Chakrapani, A.C. Pan, E. Perozo, and B. Roux. 2013. Recovery from slow inactivation in K^+ channels is controlled by water molecules. *Nature.* 501:121–124. https://doi.org/10.1038/nature12395

Pan, A.C., L.G. Cuello, E. Perozo, and B. Roux. 2011. Thermodynamic coupling between activation and inactivation gating in potassium channels revealed by free energy molecular dynamics simulations. *J. Gen. Physiol.* 138:571–580. https://doi.org/10.1085/jgp.201110670

Panyi, G., and C. Deutsch. 2006. Cross talk between activation and slow inactivation gates of Shaker potassium channels. *J. Gen. Physiol.* 128:547–559. https://doi.org/10.1085/jgp.200609644

Perozo, E., D.M. Cortes, and L.G. Cuello. 1999. Structural rearrangements underlying K^+-channel activation gating. *Science.* 285:73–78. https://doi.org/10.1126/science.285.5424.73

Phillips, J.C., R. Braun, W. Wang, J. Gumbart, E. Tajkhorshid, E. Villa, C. Chipot, R.D. Skeel, L. Kalé, and K. Schulten. 2005. Scalable molecular dynamics with NAMD. *J. Comput. Chem.* 26:1781–1802. https://doi.org/10.1002/jcc.20289

Roeper, J., C. Lorra, and O. Pongs. 1997. Frequency-dependent inactivation of mammalian A-type K^+ channel KV1.4 regulated by Ca2+/calmodulin-dependent protein kinase. *J. Neurosci.* 17:3379–3391. https://doi.org/10.1523/JNEUROSCI.17-10-03379.1997

Roux, B. 1995. The calculation of the potential of mean force using computer simulations. *Comput. Phys. Commun.* 91:275–282. https://doi.org/10.1016/0010-4655(95)00053-I

Ryckaert, J.-P., G. Ciccotti, and H.J. Berendsen. 1977. Numerical integration of the Cartesian equations of motion of a system with constraints: molecular dynamics of n-alkanes. *J. Comput. Phys.* 23:327–341. https://doi.org/10.1016/0021-9991(77)90098-5

Sadovsky, E., and O. Yifrach. 2007. Principles underlying energetic coupling along an allosteric communication trajectory of a voltage-activated K^+ channel. *Proc. Natl. Acad. Sci. USA.* 104:19813–19818. https://doi.org/10.1073/pnas.0708120104

Shaw, D.E., K.J. Bowers, E. Chow, M.P. Eastwood, D.J. Ierardi, J.L. Klepeis, J.S. Kuskin, et al.. 2009. Millisecond-Scale Molecular Dynamics Simulations on Anton.Proceedings of the Conference on High Performance Computing Networking, Storage, and Analysis, Portland, OR. doi:https://doi.org/10.1145/1654059.1654126.

Sugita, Y., A. Kitao, and Y. Okamoto. 2000. Multidimensional replica-exchange method for free-energy calculations. *J. Chem. Phys.* 113:6042–6051. https://doi.org/10.1063/1.1308516

Tilegenova, C., D.M. Cortes, and L.G. Cuello. 2017. Hysteresis of KcsA potassium channel's activation- deactivation gating is caused by structural changes at the channel's selectivity filter. *Proc. Natl. Acad. Sci. USA.* 114:3234–3239. https://doi.org/10.1073/pnas.1618101114

Uysal, S., L.G. Cuello, D.M. Cortes, S. Koide, A.A. Kossiakoff, and E. Perozo. 2011. Mechanism of activation gating in the full-length KcsA K^+ channel. *Proc. Natl. Acad. Sci. USA.* 108:11896–11899. https://doi.org/10.1073/pnas.1105112108

van der Cruijsen, E.A.W., A.V. Prokofyev, O. Pongs, and M. Baldus. 2017. Probing conformational changes during the gating cycle of a potassium channel in lipid bilayers. *Biophys. J.* 112:99–108. https://doi.org/10.1016/j.bpj.2016.12.001

Weingarth, M., E.A. van der Cruijsen, J. Ostmeyer, S. Lievestro, B. Roux, and M. Baldus. 2014. Quantitative analysis of the water occupancy around the selectivity filter of a K^+ channel in different gating modes. *J. Am. Chem. Soc.* 136:2000–2007. https://doi.org/10.1021/ja411450y

Wylie, B.J., M.P. Bhate, and A.E. McDermott. 2014. Transmembrane allosteric coupling of the gates in a potassium channel. *Proc. Natl. Acad. Sci. USA.* 111:185–190. https://doi.org/10.1073/pnas.1319577110

Xu, Y., M.P. Bhate, and A.E. McDermott. 2017. Transmembrane allosteric energetics characterization for strong coupling between proton and potassium ion binding in the KcsA channel. *Proc. Natl. Acad. Sci. USA.* 114:8788–8793. https://doi.org/10.1073/pnas.1701330114

Zhou, Y., J.H. Morais-Cabral, A. Kaufman, and R. MacKinnon. 2001. Chemistry of ion coordination and hydration revealed by a K^+ channel-Fab complex at 2.0 A resolution. *Nature.* 414:43–48. https://doi.org/10.1038/35102009